Low-Temperature Oxidative Removal of Benzene from the Air Using Titanium Carbide (MXene)-Supported Platinum Catalysts

Jiapeng Wang [a], Kumar Vikrant [a], Sherif A. Younis [a, b], Ki-Hyun Kim [a, *], Philippe M. Heynderickx [c, d]

[a] Department of Civil and Environmental Engineering, Hanyang University, 222 Wangsimni-Ro, Seoul 04763, Republic of Korea; [b] Analysis and Evaluation Department, Egyptian Petroleum Research Institute, Nasr City, Cairo 11727, Egypt; [c] Center for Environmental and Energy Research (CEER), Engineering of Materials via Catalysis and Characterization, Ghent University Global Campus, 119-5 Songdo Munhwa-ro, Yeonsu-gu, Incheon 406-840, Republic of Korea; [d] Department of Green Chemistry and Technology, Faculty of Bioscience Engineering, Ghent University, Coupure Links 653, B-9000 Ghent, Belgium.

Abstract

MXenes are an emerging class of two-dimensional (2D) inorganic materials with versatile application potentials such as adsorption and catalysis. Here, we describe the synthesis of a platinized titanium carbide MXene (Pt@Ti_3C_2) catalyst with varying amounts of platinum (0.1%–2 wt.%) for the low-temperature oxidation of benzene, an aromatic volatile organic compound often found in industrial effluent. A 1% formulation of Pt@Ti_3C_2-R achieved near-complete (97%) oxidation of benzene at 225 °C with a steady-state reaction rate (r) of 0.119 $mol \cdot g^{-1} \cdot h^{-1}$. The low-temperature catalytic oxidation of benzene to carbon dioxide was promoted by the lattice oxygen (active sites) of platinized catalysts attained through hydrogen reduction pre-treatment of Pt@Ti_3C_2-R, as revealed by X-ray photoelectron spectroscopy, temperature-programmed reduction, and in situ diffuse reflectance infrared Fourier transform spectroscopy analyses. The oxidation capability of 1% Pt@Ti_3C_2-R against benzene was assessed under the control of the key process variables (e.g., catalyst mass, flow rate, benzene concentration, relative humidity, and time-on-stream) to help optimize the catalytic oxidation process. The results provide new insights into the use of platinum-based 2D MXene catalysts for low-temperature oxidative removal of benzene from the air.

***Keywords*:** MXenes; Catalytic oxidation; Benzene; VOCs; Air pollution control

***Corresponding author: kkim61@hanyang.ac.kr (K.-H. Kim)**

1. Introduction

Industrial emissions of volatile organic compounds (VOCs) in flue gases are a major contributor to air pollution. Among various VOCs, benzene (a typical aromatic hydrocarbon) is of particular concern due to its ubiquity and recalcitrant nature. Industrial sources of benzene include petroleum refining, spraying, organic chemical production, coating, and the manufacturing of textile dyes, pharmaceuticals, leather, pesticides, printing ink, electronic equipment, and adhesives (He et al., 2019). The sources of benzene in indoor air include cosmetics, glass wool insulation, varnishes, paints, curtains, garments, disinfectants, curtains, sterilizers, wall coverings, cigarette smoke, and other consumer goods (Brdarić et al., 2019; Sekar et al., 2019). In light of the adverse health effects of benzene, a time-weighted (10 h) average exposure limit of 0.1 ppm has been fixed by the U.S. National Institute for Occupational Safety and Health (Kim et al., 2022).

Multiple treatment technologies have been developed to reduce the negative impact of VOCs in industrial effluents, including adsorption (Li et al., 2020b; Vikrant et al., 2020), absorption (Xu et al., 2021a; Lhuissier et al., 2022), membrane separation (Petrusová et al., 2019; Zhang et al., 2021), and bio-filtration (Vikrant et al., 2017; Lelicińska-Serafin et al., 2019). Among the available options, thermal catalytic oxidation is an effective and durable strategy for treating flue gases contaminated with VOCs without generating hazardous by-products (Zhang et al., 2016; Kim et al., 2022). Supported noble metal (e.g., platinum) catalysts typically display superior activity for the oxidation of most VOCs at relatively low temperatures (< 300 °C) (Zhang and Zhou, 2021). Considerable effort has been devoted to understanding how to fine-tune platinum active sites in support materials, such as metal-organic frameworks (MOFs) (Bavykina et al., 2020), activated carbon (Xu et al., 2021a), metal oxides (Kim et al., 2022), and graphene-based materials (Roy et al., 2018).

Two-dimensional (2D) layered transition-metal carbides (MXenes) have attracted considerable research interest in various applications (e.g., energy storage, catalysis, and gas sensing) (Gao et al., 2017; Kim et al., 2018; Nan et al., 2021). The number of research papers returned when searching

scientific libraries with the "MXene" keyword has grown dramatically since their first description in 2011 (Figure S1). In particular, titanium carbide (Ti_3C_2), a typical 2D MXene, is viewed as a promising active catalyst and support for noble- and transition-metal sites (e.g., platinum, cobalt, and zinc) and metal oxides (e.g., aluminum/copper(II) oxide [CuO] and titanium dioxide [TiO_2]) to accelerate catalytic reactions (e.g., photocatalysis, dehydrogenation, oxygen reduction, thermocatalysis, and electrocatalysis) (Obodo et al., 2020; Parse et al., 2021; Chu et al., 2022; Zhan et al., 2022; Cheng et al., 2023). Ti_3C_2 MXene offers abundant surface functional groups (e.g., hydroxyls) and active sites to construct a strong heterojunction with doped metal and metal oxides (Ran et al., 2017; Cai et al., 2018).

Due to the high electron conductivity of MXenes, the strong interfacial coupling between Ti_3C_2 and metal/metal oxides was found to improve the electronic structure and catalytic activity of MXene-based catalysts (Chu et al., 2022). The heterojunction formation between MXene and loaded metal could help improve charge separation to enhance the catalytic activity. For example, Ti_3C_2 nanosheets were used as support for platinum- and nitrogen-doped TiO_2 nanoparticles (NPs) to construct a 3% Pt/N-TiO_2/Ti_3C_2 heterojunction with high photocatalytic activity toward one-pot hydrogenation and amidation of nitroaromatics with carboxylic acid under visible irradiation at room temperature (RT) (Jiang et al., 2021). Ti_3C_2 MXene support for Al/CuO energetic nanocomposites significantly improved microwave combustion at low ignition temperatures in a relatively short time (Cheng et al., 2023). A Co-Zn/N-carbon (NC)-Ti_3C_2 composite catalyst was also synthesized by one-step pyrolysis of zeolitic imidazolate framework (ZIF)-67/ZIF-8 MOFs on a Ti_3C_2 surface to enhance oxygen reduction reactions in anion-exchange membrane fuel cells (Chu et al., 2022). Density functional theory analysis predicted that Ti_3C_2 MXene would be an effective catalytic support that would enhance the catalytic activity of the platinum surface toward the dehydrogenation of methylcyclohexane at elevated temperatures, relative to a pristine platinum (1 1 1) surface (Obodo et al., 2020). A platinum-supported Ti_3C_2 catalyst was also utilized for the oxidative removal of formaldehyde (oxygenated VOC) in the air at RT (Vikrant et al., 2023).

$Pt@Ti_3C_2$ composite catalysts can therefore be expected to display high activity for the low-temperature oxidative removal of aromatic VOCs from the air.

In the present study, a wetness impregnation method (WIM) was applied to dope Ti_3C_2 MXene with platinum (0.1% to 2 wt.%), followed by thermal reduction pre-treatment using hydrogen (H_2). The developed $Pt@Ti_3C_2$ catalysts were characterized and tested for their ability to oxidize benzene (a model aromatic VOC) at varying temperatures. The effect of process variables, including platinum loading, catalyst mass (m_{cat}), flow rate (FR), benzene concentration, relative humidity (RH), and time-on-stream (TOS), on the benzene oxidation reaction was also investigated in detail. The extent of benzene mineralization was quantified by measuring the amount of carbon dioxide (CO_2) produced by the catalytic reaction. In situ diffuse reflectance infrared Fourier transform spectroscopy (DRIFTS) was utilized to evaluate plausible benzene oxidation pathways. To the best of our knowledge, this study is the first to report on the application of $Pt@Ti_3C_2$ catalysts for low-temperature oxidative removal of benzene from the air.

2. Materials and methods

2.1. Materials and chemicals

Chloroplatinic acid hexahydrate ($H_2PtCl_6 \cdot 6H_2O$; ≥ 37.5% platinum basis), quartz sand (SiO_2), and benzene liquid primary standard (L-PS; ≥ 99.8%) were purchased from Sigma-Aldrich (St. Louis, Missouri, USA). Ti_3C_2 MXene powder (> 98%) was provided by Invisible Co., Ltd. (South Korea). Nitrogen (N_2; 99.999%), H_2 (99.999%), and air (99.999%) cylinders were supplied by Union Gas Co., Ltd. (South Korea).

2.2. Catalyst synthesis

Platinum (0.1 wt%, 1 wt%, and 2 wt.%)@Ti_3C_2 MXene catalysts were synthesized using an IMP protocol described previously (Vikrant et al., 2023). In brief, $H_2PtCl_6 \cdot 6H_2O$ (3.8, 38, or 76 mg) was dissolved in 20 mL of deionized (DI) water (H_2O) under stirring for 15 min. Subsequently, 1 g of Ti_3C_2 was added to the prepared platinum solution and stirred for another 24 h at RT. The obtained suspensions were then transferred to a convection oven (ED-CO150, Han Yang Scientific Equipment Co., Ltd., South Korea) heated to 85 °C (15 h) to yield the 0.1 wt%, 1 wt%, and 2 wt% Pt@Ti_3C_2 catalysts. The instrumental characterization of the synthesized catalysts is detailed in the Supplementary Information (SI).

2.3. Temperature-programmed reduction

Temperature-programmed reduction (TPR) using hydrogen and carbon monoxide (CO) experiments were performed to characterize the tested materials with an AutoChem II (Micromeritics Instrument Corp., Norcross, Georgia, USA) apparatus. For these experiments, 80.4 ± 0.2 mg of 1%Pt@Ti_3C_2 and 1%Pt@Ti_3C_2-R ("R" indicates reduction pre-treatment) catalysts were treated by a flow (FR of 20 mL min^{-1}) of molecular oxygen (5% in argon) at a heating rate of 10 K min^{-1} up to 383.2 K for activation and removal of weakly adsorbed species (CO_2 and H_2O). The treated samples were cooled to 303.2 K under a 50 mL min^{-1} argon flow to remove all physically adsorbed oxygen. TPR was carried out under a flow of H_2 or CO in helium (0.10 mol mol^{-1} and a total FR of 50 mL min^{-1}) at 10 K min^{-1} up to 1,073 K and a constant pressure of 107.1 ± 1.2 kPa. During H_2-based TPR analysis, the reactor outlet was subcooled using isopropyl alcohol at −80 °C to avoid the signal distortion of the thermal conductivity detector (TCD) by the formed H_2O. During the CO-based TPR analysis, the TCD outlet signal was corrected for the formation of CO_2 using the difference in thermal conductivity (SI).

2.4. Catalytic activity

For the catalytic experiment, three doses of the prepared catalysts (e.g., 2, 10, and 30 mg) were physically mixed with SiO_2 (at a fixed weight ratio of 1:5) and packed in quartz tubes (90 × 4 mm) between two layers of quartz wool. The fixed-bed catalyst tubes were pre-treated for 180 min at 300 °C in an electric tube heater (model TC200P (K), Misung Scientific Co., Ltd., South Korea) under a flow of 10% H_2/N_2 to reduce the catalyst and remove the pre-adsorbed moisture (Argyle and Bartholomew, 2015; Matsumoto et al., 2020). The benzene (547.9 ppm: assuming 100% recovery) gaseous primary standard (G-PS) was prepared by injecting 4 μL of the benzene L-PS into a 2 L polyester aluminum (PEA) bag (Top Trading Co., Ltd., South Korea) filled with N_2. The PEA bag was then left to stand under ambient conditions overnight to ensure complete vaporization and stabilization of the benzene vapor. The obtained G-PS of benzene was then diluted with air in a 20 L PEA bag to prepare a benzene gaseous working standard (G-WS) of varying concentrations (1 to 100 ppm). For the experiments conducted in the presence of moisture, suitable amounts of DI H_2O were injected into the benzene G-WS PEA bags to obtain an RH between 0% and 80% by following the procedure described by works (Liu et al., 2021; Tran et al., 2022)).

A schematic for the experimental setup for the catalytic oxidation of benzene is presented in Figure 1. The benzene G-WS PEA bag was connected to the reactor inlet while the outlet was linked to a mini pump (MP-Σ300NII, Sibata, Japan) for pulling the G-WS through the catalyst bed at a fixed FR of 300 mL min^{-1}. An online gas chromatograph–flame ionization detector equipped with a methanizer system (iGC-7200, DS Science Inc., South Korea) and a large-volume injector (PRG-2010, Shimadzu, Japan) were used to quantify the benzene and CO_2 generated during the catalytic reaction at different time intervals. During the thermocatalytic reaction, the reaction temperature increased at intervals of 25 °C until oxidation of benzene vapor in the gaseous flow was complete. Measurements of benzene conversion ($R_{benzene}$, %) and the steady-state reaction rate (r, mol $g^{-1} \cdot h^{-1}$) were employed to evaluate the catalytic performance (Vikrant et al., 2021; Kim et al., 2022; Vikrant et al., 2022) (Equation 1). The

value of r was computed using Equation 2 to evaluate the rate of chemical reaction on the catalyst surface. $F_{benzene}$ represents the benzene flowrate (mol s^{-1}).

The r calculated using Equation 2 is only valid when the reactor operates under differential conditions, i.e., $R_{benzene} < 20\%$. Under the differential mode of operation, the reactant partial pressures remain constant along the fixed bed quartz tube reactor. Hence, the benzene disappearance rate ($-r_B$) remains constant under differential conditions inside the fixed bed reactor, irrespective of the position. The r calculated using Equation 2 overestimates the true r under integral conditions, i.e., $R_{benzene} > 20\%$. As the governing kinetic model and parameters were not derived in the present work, a simple r calculation using Equation 2 was utilized for the performance comparison between similar experiments in relative sense. (It should hence be noted the r obtained under integral conditions can overestimate the actual performance.)

$$R_{benzene}(\%) = \frac{(\text{benzene peak area})_{in} - (\text{benzene peak area})_{out}}{(\text{benzene peak area})_{in}} \times 100 \qquad \text{(Equation 1)}$$

$$r = \frac{3{,}600 \times 10^3 \times R_{benzene} \times F_{benzene}}{m_{cat}} \qquad \text{(Equation 2)}$$

2.5. Light-off curves

The steady-state continuity equation for compound "i" in a packed-bed reactor is given by Equation 3, where X_B, $F_{B,0}$, and $r(X_B)$ represent the benzene conversion ($mol_B \cdot mol_{B,0}^{-1}$), the inlet molar flow rate of benzene ($mol_{B,0} \cdot s^{-1}$), and the reaction rate for benzene total oxidation ($mol_B \cdot kg_{cat}^{-1} \cdot s^{-1}$), respectively.

$$\frac{dX_B}{d\, m_{cat}/F_{B,0}} = r\left(X_B\right) \qquad \text{(Equation 3)}$$

The "space-time" ratio $m_{cat}/F_{i,0}$ (Heynderickx et al., 2009, 2010a) is expressed in $kg_{cat} \cdot s \cdot mol_{i,0}^{-1}$. The apparent first-order reaction rate is calculated using Equation 4. The inlet O_2 concentration was approximately 2,000 times greater than the inlet VOC concentration in the present work. The O_2 concentration was therefore assumed to remain constant, and the reaction was assumed to proceed in the

first order (concerning the substrate concentration) (Zhang et al., 2020; Zhao et al., 2021). The compound concentration can be related to the conversion efficiency and the corresponding inlet concentration, as described in Equation 5. The relationship between the conversion and space-time ratio is given in Equation 6.

$$r = k_{app} C_B \qquad \text{(Equation 4)}$$

$$C_B = C_{B,0} \cdot \left(1 - X_B\right) \qquad \text{(Equation 5)}$$

$$X_B = 1 - \exp\left(-k_{app} \cdot C_{B,0} \cdot \frac{m_{cat}}{F_{B,0}}\right) \qquad \text{(Equation 6)}$$

If the concentration for compound "i" is expressed in $mol_B\ m^{-3}$, the units of k_{app} (and also $k_{app,\infty}$) is $m^3\ kg_{cat}^{-1}\ s^{-1}$. Equation 7 converts ppm_B into $mol_B\ m^{-3}$ by assuming that the inlet flow conditions are established at RT. (24.464 is molar volume of gas (L mol^{-1}) at 25 ºC)

$$\left(C_B\right) = \left(ppm_B\right) \cdot \frac{10^{-3}}{24.464} \qquad \text{(Equation 7)}$$

For different isotherm conditions, the so-called "light-off curve" can be constructed based on Equation 6, where the conversion versus temperature can be considered using the Arrhenius relation (Equation 8).

$$k_{app} = k_{app,\infty} \cdot \exp\left(-\frac{E_{app}}{RT}\right) \qquad \text{(Equation 8)}$$

The pre-exponential factor ($k_{app,\infty}$) and the apparent activation energy (E_{app}) are obtained from non-linear parameter estimates (Section S4), using the complete conversion versus temperature data set per catalyst: see Figure 2. The value of $k_{app,\infty}$ in the first-order reaction coefficient ($m_f^3\ kg_{cat}^{-1}\ s^{-1}$) can be converted into s^{-1} through Equation 9, using the catalyst porosity, ε_p ($m_f^3\ kg_{pellet}^{-1}$; where "f" denotes free space and "pellet" refers to the catalyst, including the pores).

$$k'_{app,\infty} = k_{app,\infty} \cdot \frac{\rho_{cat}\left(1-\varepsilon_p\right)}{\varepsilon_p} = k_{app,\infty} \cdot \frac{2}{r_{p,av} \cdot S} \qquad \text{(Equation 9)}$$

The units for the conversion are ($kg_{cat}\ m_{cat}^{-3} \cdot m_{cat}^{3}\ m_{pellet}^{-3}$)/($m_f^3\ m_{pellet}^{-3}$) = $kg_{cat}\ m_f^{-3}$ (Section S5). For an irreversible reaction, the relationship between the pre-exponential factor ($k'_{app,\infty}$: s^{-1}) and $\Delta S^{\ddagger}$ (entropy difference between the activated complex and reactants) is given by Equation 10.

$$k'_{app,\infty} = \frac{k_B T}{h} \exp\left(\frac{\Delta S^{\neq}}{R}\right) \qquad \text{(Equation 10)}$$

The $\Delta S^{\neq}$ value contributes to the shift in equilibrium between the reactants and the activated complex through the usual thermodynamic relationship $\Delta G^{\neq} = \Delta H^{\ddagger} - T \cdot \Delta S^{\ddagger}$ (Vyazovkin, 2021). A positive value for $\Delta S^{\ddagger}$ suggests that entropy increases upon achieving the transition state, which often indicates a dissociative mechanism in which the activated complex is loosely bound. Negative values for $\Delta S^{\ddagger}$ indicate that entropy decreases on forming the transition state, which often indicates an associative mechanism in which two reaction partners form a single activated complex (Espenson, 1981; Akram et al., 2016).

3. Results and discussion

Direct thermocatalytic oxidation is an efficient technique for removing aromatic VOCs (e.g., benzene) from gaseous streams (air and flue gas). In the present section, the effect of high-temperature H_2 reduction is evaluated with respect to the low-temperature catalytic behavior of Pt@Ti_3C_2 against benzene. In addition, the catalytic performances were studied at various process variables (e.g., platinum loading, m_{cat}, FR, benzene concentration, RH, and TOS). Figure 2 plots the light-off curves of the

benzene oxidation reaction to emphasize the differences in catalytic efficiency between the comparable systems and the effect of platinum loading.

3.1. Effect of high-temperature H_2 reduction pre-treatment on the activity of Pt@Ti_3C_2 catalysts

To study the effect of pre-treatment on the catalyst, Figure 2(a) presents the light-off curves for a benzene oxidation reaction over a 1% Pt@Ti_3C_2 catalyst (relative to pristine Ti_3C_2 MXene as a "carrier/support") before and after H_2 reduction "R" pre-treatment. The 1% formulation of Pt@Ti_3C_2-R achieved higher catalytic activity compared with 1% Pt@Ti_3C_2 and pristine Ti_3C_2-R, as shown in Figure 2(a). From the calculated performance metrics in Table 1, 1% platinum catalysts exhibited the highest catalytic activity against benzene vapor at 200–225 °C. At 200 °C, the r value for benzene over 1% Pt@Ti_3C_2-R was 0.012 $mol \cdot g^{-1} \cdot h^{-1}$, approximately 1.71 to 12 times higher than that for 1% Pt@Ti_3C_2 (0.007 $mol \cdot g^{-1} \cdot h^{-1}$) and Ti_3C_2-R (0.001 $mol \cdot g^{-1} \cdot h^{-1}$). The reduction pre-treatment of the platinum-loaded Ti_3C_2 catalyst under high-temperature H_2 flow therefore had a significant promotional effect on the catalytic performance due to support strong metal-support interaction, i.e., facile transfer of electrons at the Pt-MXene interface (Cui et al., 2020; Li et al., 2022).

The reduction pre-treatment was found to increase the amount of mobile lattice oxygen (vacant oxygen centers) while decreasing the chemisorbed oxygen (O_{II}) over the reduced catalysts (as validated later by X-ray photoelectron spectroscopy (XPS). The platinum metal sites can promote the activation of vacant oxygen sites and O_{II} species on the catalyst surface to synergistically interact with adsorbed benzene molecules and accelerate the diffusion of active oxygen species (O*) from the subsurface or bulk layers (Yang et al., 2020; Rosli et al., 2022). The catalytic activity of Ti_3C_2-R can be ascribed to the reaction between the benzene molecules and the O* on the surface at elevated temperatures as shown in Figure S10(a). The consumed O* could be replenished by the O_2 in the reaction atmosphere (Sun et al.,

2015). As a result, platinum loading onto Ti_3C_2 and H_2 reduction pre-treatment of Pt@Ti_3C_2 can synergistically improve the catalytic activity involved in benzene oxidation at low temperatures.

3.2. Effect of platinum loading and reaction temperature

The effect of platinum loading (0.1 wt.%, 1 wt.%, and 2 wt.%) on low-temperature benzene oxidation was assessed using Pt@Ti_3C_2-R, as seen in Figure 2(b). The most active catalyst at low temperatures, 2% Pt@Ti_3C_2-R, completely oxidized the benzene (the temperature at 100% $R_{benzene}$ (T_{100}) = 200 °C). In contrast, the T_{100} increased to 225 °C and 350 °C when platinum loading was decreased to 1 wt.% and 0.1 wt.%, respectively (Table 1). However, both 2% and 1% Pt@Ti_3C_2-R displayed the same r (0.012 mol g^{-1} h^{-1}) at 200 °C, which was 2.4 and 12 times greater than those obtained by 0.1% Pt@Ti_3C_2 (0.005 mol g^{-1} h^{-1}) and Ti_3C_2 (0.001 mol g^{-1} h^{-1}), respectively (Table 1). The as-prepared 1% Pt@Ti_3C_2-R had the highest E value (Table S2), although it also had the highest k value. For r per m_{cat}, 1% Pt@Ti_3C_2-R (0.012 mol g_{cat}^{-1} h^{-1}) and 2% Pt@ Ti_3C_2-R (0.012 mol g_{cat}^{-1} h^{-1}) performed better than other catalysts (Table 1). For the r per Pt mass, 0.1% Pt@Ti_3C_2-R (3.96 mol g_{cat}^{-1} h^{-1}) was the best performer (Table 1).

In Table S2, the positive value of $\Delta S^{\ddagger}$ (16.3 ± 9.8 kJ mol^{-1} K^{-1}) between the activated complex and reactants for the 1% Pt@Ti_3C_2-R catalyst may comply with higher mobility of the surface oxygen species, resulting in a more straightforward oxidation reaction by inserting O* species. However, the 0.1% Pt@Ti_3C_2-R catalyst had a low E and a non-favorable activated complex: see Equation (10). (As the surface reaction intermediate(s) can be considered to be more tightly fixed to the catalyst surface, it is less prone to further oxidation or total oxidation product formation such as H_2O and CO_2.) Lastly, the 2% Pt@Ti_3C_2-R catalyst displayed an active complex with a near-zero $\Delta S^{\ddagger}$ value. In this case, the activated complex for total oxidation (the surface intermediate(s)) may have an entropy value comparable to the reactants. ~~The entropy difference can reflect the adsorption behavior of benzene onto~~

~~the catalyst surface. Strong adsorption is accompanied by a substantial reduction in entropy of the benzene surface species, whereas weak adsorption exhibits the opposite behavior.~~ Although 2% Pt@Ti_3C_2-R outperformed all the other tested catalysts for low-temperature benzene oxidation, 1% Pt@Ti_3C_2-R was selected for further study due to its lower cost and the similarity of its catalytic activity to that of the 2% catalyst in the 200–225 °C range.

3.3. TPR results

The role of reduction pre-treatment in catalytic activity was evaluated using TPR analysis (Figures 3 and 4). Table S3 summarizes the corresponding TPR data of 1% Pt@Ti_3C_2 (relative to Ti_3C_2) as a function of temperature. The peak temperatures can be considered a measure of surface reducibility: the smaller the temperature, the easier it is to consume the corresponding active oxygen surface species. The occurrences of weakly bonded species (O^{2-}, O^{-}…) were seen with low(er) reduction temperatures (Panov et al., 2006). In contrast, the lattice oxygen consumption for reduction normally corresponded to high(er) reduction temperatures. (In this case, the oxygen is part of a lattice to consume more energy.) As approximately 80 mg of the catalyst is commonly used in TPR experiments, the total available surface oxygen (C_o: $mol_O\ kg_{cat}^{-1}$) can be approximated as 10^{-1} $mol_O\ kg_{cat}^{-1}$ during reduction (entries 1 and 4 in Table S3). These values were comparable to those obtained through TPR analysis of other metal-oxide catalysts studied previously (Heynderickx et al., 2010b).

3.3.1. CO-based TPR and H_2-based TPR

In the present study, 1% Pt@Ti_3C_2 and 1% Pt@Ti_3C_2-R exhibited significantly higher oxygen storage capacities during CO-based TPR and H_2-based TPR analyses than did Ti_3C_2. In the case of the CO-based TPR, reduction pre-treatment of 1% Pt@Ti_3C_2 achieved a slight improvement, increasing the C_o value

from 4.13 ± 0.04 to 4.84 ± 0.03 $mol_O\ kg_{cat}^{-1}$ for 1% Pt@Ti_3C_2 and 1% Pt@Ti_3C_2-R, respectively (Table S3). Comparatively, the C_o value of the 1% Pt@Ti_3C_2-R catalyst (4.44 10^{-1} $mol_O\ kg_{cat}^{-1}$) was 1.5 times higher than that of the 1% Pt@Ti_3C_2 catalyst (2.97 10^{-1} $mol_O\ kg_{cat}^{-1}$) under H_2-based TPR analysis (Table S3). The possible reason for the higher oxygen uptake can be attributed to the prior reduction of platinized catalysts by H_2, followed by reoxidation during the synthesis of 1% Pt@Ti_3C_2-R. As oxygen is removed during reduction pre-treatment at high temperatures, it can be removed rapidly in the subsequent reduction experiment. In contrast, the 1% Pt@Ti_3C_2 catalyst removed considerably fewer oxygen atoms, as it did not go through a prior reduction treatment.

The occurrences of multiple reduction peaks in the low- and high-temperature ranges in the H_2-based TPR and CO-based TPR profiles (Figure 3) indicate the presence of different oxygen-containing groups (e.g., OH) on the as-prepared platinized MXene catalysts. In the case of the CO-based TPR analysis, reduction peaks for the Ti_3C_2 carrier were observed between 170 °C and 350 °C. In contrast, the reduction peaks for the 1% Pt@Ti_3C_2 and 1% Pt@Ti_3C_2-R catalysts appeared between 120 °C and 560 °C. During the H_2-based TPR analysis, the temperature for H_2 reduction was much higher than that for CO for the Ti_3C_2 MXene carrier. However, lower reduction temperatures were observed for the first reduction peak in the case of the Pt@Ti_3C_2 catalysts. In particular, reduction peaks in the H_2-based TPR profiles (Figure 3) of the Ti_3C_2 carrier and Pt@Ti_3C_2 catalysts were observed in temperature ranges of 170 °C to 600 °C and 40 °C to 550 °C, respectively. These observations indicate the formation of additional reducible surface oxygen species due to doped platinum atoms on the MXene surface.

As can be seen in the CO-based TPR profiles (Figure 3), the low-temperature peaks (below 350 °C) contributed to a significant percentage (e.g., 62% and 91%) of the total signal for the 1% Pt@Ti_3C_2 and 1% Pt@Ti_3C_2-R catalysts, respectively. The additional peaks at higher temperatures (> 350 °C: compared to the carrier material) contributed approximately 38% and 9% of the total signal for 1% Pt@Ti_3C_2 and 1% Pt@Ti_3C_2-R, respectively. However, the first reduction peak for the Ti_3C_2 carrier was

observed at a higher temperature (191.6 °C) compared with 1% Pt@Ti_3C_2 (158.4 °C). The peak reduction temperature for 1% Pt@Ti_3C_2-R was relatively high (222.1 °C). The enhanced contribution of the first peak for 1% Pt@Ti_3C_2 (20% relative to 7% recorded by 1% Pt@Ti_3C_2-R) in the total signal of reducible oxygen atoms could explain the superior activity of the latter. The greater oxygen concentration available for reduction could also explain the synergistic role of reduction pre-treatment in the enhanced performance of Pt@Ti_3C_2-R (relative to the Ti_3C_2 MXene carrier and Pt@Ti_3C_2). Because a similar amount of oxygen was used for the reduction with CO (33.1 ± 3.3 and 39.1 ± 2.5 μmol_O), reduction treatment at the catalyst preparation stage may lead to a significant shift of O* species toward lower reduction temperatures.

According to the H_2-based TPR analysis, the first peak reduction temperature for 1% Pt@Ti_3C_2-R (106.9°C) was significantly higher than that for 1% Pt@Ti_3C_2 (67.7°C), while it was 2.5-fold lower than that for the Ti_3C_2 carrier (269.5 °C). The reducible oxygen atom for 1% Pt@Ti_3C_2-R was approximately 17%, which was 3.4 times higher than that for 1% Pt@Ti_3C_2. This observation may explain the superior activity of 1% Pt@Ti_3C_2-R compared with 1% Pt@Ti_3C_2, and the MXene support at low temperatures. Besides, the high-temperature peaks (> 350 °C) decreased after platinum deposition (from approximately 70% to 6% and 11%, as shown in Table S3). Three peaks were observed for Ti_3C_2 in the high-reduction-temperature region, whereas only two were observed for the platinum catalysts (Figure 3). An extra peak was observed for the platinum catalysts in the lower-temperature region. Interaction with the deposited platinum may have caused a shift in reduction temperature, lowering the corresponding surface oxygen concentration.

3.3.2. Effect of reduction pre-treatment on the catalytic activity

325 A linear relationship was found in the peak reduction temperatures of both CO-based TPR and H_2-
326 based TPR data between the 1% Pt@Ti_3C_2-R and the 1% Pt@Ti_3C_2 as can be seen in Figure 4 (a). The
327 reduction temperatures appeared to be higher for the former until approximately 400 °C, while such a
328 pattern was reversed at higher temperatures. As a benzene aromatic ring contains more electrons
329 compared with CO or H_2, the overall reaction may be subject to the complicated effects of adsorption
330 (benzene + O_2) and surface reactions. For example, if the peak temperatures for both catalysts are
331 compared relative to the Ti_3C_2 carrier (ranked in increasing order), CO should require equal or higher
332 reduction temperatures. In contrast, the opposite result should be obtained for H_2-based TPR, i.e., lower
333 reduction temperatures for the platinum catalysts, as shown in Figure 4 (b) and (c). For the results of
334 CO-based TPR, the Ti_3C_2 carrier appears to achieve superior reducibility at lower temperatures
335 compared with platinum catalysts. Instead, the opposite H_2-based TPR results suggest that, due to the
336 complexity of surface catalysis, the performance of catalysts cannot be analyzed by a single
337 characterization. It is better to characterize the catalysts by combining other methods (e.g., XPS and in
338 situ DRIFTS) with TPR. Because the best-performing catalyst achieved a higher reduction temperature
339 for the first peak (H_2 and CO reduction), benzene adsorption and activation, rather than oxygen
340 consumption in VOC oxidation, is likely the rate-determining step of the overall reaction.

341

342 *3.4. Effect of process variables on catalytic activity*

343 *3.4.1. Effect of m_{cat} and flow rate*

344 The effect of 1% Pt@Ti_3C_2-R m_{cat} (2, 10, and 30 mg) on the oxidation of benzene vapor at 225 °C
345 can be assessed as a function of reaction time. As seen in Figure 5(a), $R_{benzene}$ increased from 75% to
346 100% at 225 °C upon increasing the m_{cat} from 2 to 30 mg. The value of r increased from 0.004 to 0.046
347 mol g^{-1} h^{-1} with a decrease in m_{cat} from 30 to 2 mg (Table S4). The decreased activity with increased m_{cat}
348 was likely due to a lowering of the utilization efficiency of the active sites of the catalysts. If the m_{cat}

was 10 mg, $R_{benzene}$ decreased gradually from 99% to 96% with an increasing FR (50 to 200 mL min^{-1}), as shown in Figure 5(b) (Wang et al., 2019). However, r increased from 0.012 to 0.047 mol g^{-1} h^{-1} with an increase in the FR (Table S4). The increased catalytic activity at a higher FR suggests that more benzene molecules reacted with the active sites on the Pt@Ti_3C_2-R surface.

3.4.2. Effect of benzene concentration and RH

The catalytic activity of 1% Pt@Ti_3C_2-R was further studied as a function of varying benzene concentrations (2 to 100 ppm) and RH levels (0 to 80%). Figure 5(c) shows that $R_{benzene}$ increased from 90.8% to 99% upon increasing the inlet benzene concentration from 2 to 10 ppm. Increasing the inlet benzene concentration another 10-fold showed no significant effect on $R_{benzene}$, which was 99.4% and 97.3% at 50 and 100 ppm benzene, respectively, even after 210 min TOS. The increase in r from 0.002 to 0.119 mol g^{-1} h^{-1} with the increase in benzene concentration from 2 to 100 ppm can be attributed to an increase in the utilization efficiency of the active sites on the catalyst surface (Table S4).

Figure 5(d) shows the CO_2 detected upon catalytic oxidation of benzene at the highest (100 ppm) and lowest (2 ppm) tested concentrations. At 225 °C, the thermocatalytic oxidation of 100 and 2 ppm benzene over 1% Pt@Ti_3C_2-R yielded 648 and 29 ppm of CO_2 production after 210 min TOS, with corresponding Y_{CO_2} values of 108 and 242%, respectively, as shown in Figure 5(d). These measured CO_2 values were higher than the expected CO_2 yield (600 and 12 ppm, respectively). If the inlet benzene vapor has been entirely mineralized for CO_2, the balanced equation should be $2C_6H_6 + 15O_2 \rightarrow 12CO_2 + 6H_2O$. These findings suggest that the mineralization of surface-accumulated benzene molecules with reaction time should yield excess CO_2 in the effluent (Xu et al., 2021b; Vikrant et al., 2022).

It is critical to evaluate the effect of RH (0%, 50%, and 80%) on the benzene oxidation performance of 1% Pt@Ti_3C_2-R at 225 °C due to the ubiquity of moisture in real-world conditions, as depicted in Figure 5(e). Compared with a dry gas stream (0% RH), the presence of water vapor (50% and 80% RH)

373 significantly suppressed the catalytic activity of 1% Pt@Ti_3C_2-R toward benzene oxidation ($R_{benzene}$
374 value of 5.1%–8.9%) at the beginning of the thermocatalytic reaction process (TOS = 0–50 min). After
375 50 min TOS, the catalytic activity of 1% Pt@Ti_3C_2-R rapidly recovered at all tested RH levels. $R_{benzene}$
376 values were 93.4% and 91.6% at 50% and 80% RH, respectively. A steady state was maintained even
377 after 210 min TOS at 225 °C. In addition, the values of r displayed a slight decline of 0.08% from dry
378 (0% RH) to humid (50% and 80% RH) conditions (Table S4), indicating that moisture had a slight
379 inhibitory effect on the catalytic activity of Pt@Ti_3C_2-R. The catalyst also exhibited acceptable
380 reusability without alteration in the catalytic activity even after seven reuse cycles under dry conditions
381 (0% RH), as shown in Figure 5(f).

382 The initial drop in the catalytic activity of 1% Pt@Ti_3C_2-R under humid conditions is likely explained
383 by competition among H_2O, benzene, and O_2 molecules for active surface sites (Liu et al., 2019; Yang
384 et al., 2019; Kong et al., 2020; Saqlain et al., 2021). With an increase in the TOS at 225 °C, the oxygen
385 vacancies (lattice oxygen) on the catalyst surface may be activated, initiating the desorption and
386 activation of H_2O and O_2 reactants and generating reactive oxidative species for benzene oxidation. The
387 thermocatalytic oxidation over Pt@Ti_3C_2-R may therefore eliminate aromatic VOCs under real-world
388 conditions in dry and moist environments at low temperatures.

389

390 *3.4.3. Pt@Ti_3C_2-R catalytic stability*

391 The catalytic stability of 2 mg of 1% Pt@Ti_3C_2-R was explored under dry conditions at 200 °C against
392 10 ppm benzene and an FR of 50 mL min^{-1}. As shown in Figure 6, the catalyst maintained high stability
393 and durability, with less than a 6% reduction in catalytic activity over 5 h TOS. The low-temperature
394 catalytic process may be the primary reason for the prolonged survival of the catalyst under oxidizing
395 conditions. The tested catalyst therefore appears to be sufficiently robust for the oxidative removal of
396 benzene under real-world conditions.

397 Transmission electron microscope (TEM) images and selected area electron diffraction (SAED)
398 analyses indicated no significant changes in morphology and an average particle-size distribution of 1%
399 Pt@Ti_3C_2-R when a comparison was made between before (9 ± 0.32 nm) and after 5 h (7.85 ± 0.17 nm)
400 of TOS oxidation reactions (Figure S13). However, powder X-ray diffraction (PXRD) patterns of the
401 spent 1% Pt@Ti_3C_2 catalyst, when compared with the fresh catalyst, exhibited significant changes after
402 benzene oxidation, as depicted in Figure S4 and Figure S13(d). Specifically, after oxidation, the intensity
403 of the 2θ diffraction peaks for MXene at 18.62° and 60.93° increased, whereas the intensity of the 2θ
404 diffraction peaks for Pt_3Ti at 25.26°, 48.14°, 54.69°, 68.59°, and 76.45° decreased. Such observations
405 may be attributable to poor crystallinity caused by the accumulation of strongly bounded by-products
406 on the catalyst surface (Kumar et al., 2018).

407 According to the XPS data for 1% Pt@Ti_3C_2-R after 5 h TOS shown in Figure S14(a), the Ti 2p
408 spectrum can be deconvoluted into four peaks at 459.5 (Ti-C), 461.22 (Ti^{3+}), 465.19 (Ti^{4+}), and 472.4
409 eV (satellite peak) (Konstantinova et al., 2018). The peaks for Ti-C, Ti^{3+}, and Ti^{4+} showed slight shifts
410 toward lower binding energy (−0.09 to −0.61 eV) compared with those observed for fresh 1% Pt@Ti_3C_2-
411 R, possibly due to the reduction of titanium species under continuous heating at 200 ℃ during the
412 reaction (Jiang et al., 2007). In the case of the C 1s spectrum in Figure S14(b), the C 1s core level can
413 be deconvoluted into four peaks at 284.64 (C-Ti), 285.7 (C-C), 287.13 (C-O), and 289.65 eV (O-C=O),
414 with slight blue shifts compared to fresh 1% Pt@Ti_3C_2-R. The blue shifts in the binding energies may
415 reflect the effects of chemical interactions between the catalyst and the benzene molecules (Li et al.,
416 2020a).

417 In Figure S14(c), deconvolution of the O 1s spectrum yields two peaks at 531.09 and 532.78 eV,
418 corresponding with Ti-O (O*) and C-Ti-$(OH)_x$/H_2O_{ads}/O_{ads} (adsorbed oxygen), respectively. The amount
419 of O* in 1% Pt@Ti_3C_2-R increased from 45.3% to 71% after reduction pre-treatment. However, the
420 amount of O* in the catalyst decreased to 63% after benzene oxidation (Table S5). These findings are

consistent with the experimental results shown in Figure 2(a) and Figure 6. For the Pt 4f spectrum in Figure S14(d), four peaks were observed at 72.27 ($4f_{7/2}$ Pt^0), 73.37 ($4f_{7/2}$ Pt^{2+}), 75.82 ($4f_{5/2}$ Pt^0), and 78.59 eV ($4f_{5/2}$ Pt^{2+}). The XPS analysis of the catalyst after benzene oxidation also produced a new peak (for the Pt^{2+} species), with a blue shift for other peaks due to the intrinsic charge transfer after 5 h TOS. Similarly, the amount of Pt^{2+} in the catalyst increased from 34.6% to 61.7% after reduction pre-treatment. However, the amount of Pt^{2+} in the catalyst decreased to 40.5% after benzene oxidation (Table S5), which is consistent with the experimental results shown in Figure 2(a) and Figure 6. The platinum clusters and NPs dispersed on the Ti_3C_2 surface during thermal reduction pre-treatment at 300 °C to form more Pt^{2+} species (Figure S2) (Poerwoprajitno et al., 2022). Combined with the experimental results depicted in Figure 2(a), the Pt^{2+} species may have catalyzed benzene oxidation more favorably than the Pt^0 (Guo et al., 2020).

3.5. Reaction mechanism and pathway

In situ DRIFTS was conducted to evaluate the benzene oxidation pathway and mechanism for 1% Pt@Ti_3C_2-R at varying temperatures from RT to 300 °C. As seen in Figure 7, similar intermediates were observed in the DRIFTS spectra for benzene (250 ppm) oxidation over 1% Pt@Ti_3C_2-R across varying temperatures (RT–300 °C). The reaction temperature therefore did not alter the benzene oxidation pathway. The DRIFTS spectra produced prominent bands for (i) formate (1528 cm^{-1}), (ii) phenolate (1595 cm^{-1}), (iii) C=O vibration of benzoquinone (1703 cm^{-1}), and (iv) adsorbed H_2O and surface OH (3647-3880 cm^{-1}) (Qin et al., 2020; Kim et al., 2022). The benzene ring first adsorbs on the surface of the catalyst. The O* (active sites) on the catalyst surface induce oxidation to generate oxygen vacancies, which can be replenished by O_2 molecules adsorbed dissociatively on the platinum active sites (Sun et al., 2015). Benzene oxidation by O* forms phenolate species, followed by a ring-opening reaction to

444 produce smaller aliphatic intermediates (e.g., formate). Eventually, the synergistic interaction between
445 O* and platinum on the MXene surface promotes the conversion of formate to CO_2 and H_2O.

446

447 *3.6. Catalytic performance comparison*

448 The results obtained in the present work were compared with those reported previously (including
449 the supported platinum and other catalysts) to assess catalytic performance differences (Table S6). The
450 value of r at T_{100} was used as the critical metric to compare catalytic performance based on an earlier
451 recommendation (Vikrant et al., 2022). We observed that the 1% Pt@Ti_3C_2-R used in the present study
452 could attain 100% $R_{benzene}$ at a relatively lower temperature (225 °C) compared with some of the
453 previously reported catalysts (Deng et al., 2018; Guo et al., 2019; Sophiana et al., 2020; Liu et al., 2021).
454 Similarly, the r-value of 0.119 mol g^{-1} h^{-1} for 1% Pt@Ti_3C_2-R was higher than that of most previously
455 reported catalysts for low-temperature benzene oxidation (Shim and Kim, 2010; Li et al., 2016; Zhu et
456 al., 2017; Zhang et al., 2018). In general, the supported platinum catalysts outperformed other catalysts
457 (e.g., manganese-based catalysts) for the oxidation of benzene (Huang et al., 2015).

458

459 **4. Conclusions**

460 In the present work, platinum-loaded 2D Ti_3C_2 MXene catalysts were synthesized by a one-pot IMP
461 for benzene oxidation at varying operating conditions (e.g., reaction temperature, platinum loading, m_{cat},
462 benzene concentration, FR, and RH). The catalytic oxidation activity of the platinized catalyst
463 (Pt@Ti_3C_2) was improved through reduction pre-treatment using H_2. The catalytic activity was further
464 enhanced by increasing the platinum loading from 0.1 wt.% to 1 wt.%. Specifically, the 1% Pt@Ti_3C_2-
465 R was the best candidate for completely oxidizing benzene (10 ppm) to CO_2 at 225 °C under dry
466 conditions. At 225 °C, the value of r decreased in the order of 1% Pt@Ti_3C_2-R (0.012 mol g^{-1} h^{-1}) > 1%
467 Pt@Ti_3C_2 (0.007 mol g^{-1} h^{-1}) > Ti_3C_2-R (0.001 mol g^{-1} h^{-1}). Moisture was found to exert inhibitory effects

on the catalytic oxidation of benzene, especially at the initial reaction stage. In contrast, catalytic activity recovered for an extended reaction time at 225 °C to produce a $R_{benzene}$ > 90% at 50%–80% RH after 210 min TOS. The reusability study also proved the high catalytic oxidation stability of 1% Pt@Ti_3C_2-R over seven cycles when tested for 300 min TOS. Based on the results of XPS, TPR, and in situ DRIFTS analyses, we postulated that the surface O* active sites attacked the adsorbed benzene ring on the 1% Pt@Ti_3C_2-R surface, inducing a series of thermal oxidation reactions and generating various intermediates (phenolates and formate) that subsequently oxidized to CO_2 and H_2O as end products. The present work demonstrates the significant potential of platinized MXene for the effective oxidation of gaseous benzene at lower temperatures. The results of this study are expected to open a path for a better understanding of the role of the platinum-loaded 2D Ti_3C_2 MXene catalysts during benzene oxidation.

Acknowledgments

This work was supported by a grant from the National Research Foundation of Korea (NRF) funded by the Ministry of Science and ICT (MSIT) of the Korean government (Grant No.: 2021R1A3B1068304). P.M.H. would like to thank the Research and Development Program of Ghent University Global Campus (GUGC), Korea.

References

Akram, A., Freakley, S.J., Reece, C., Piccinini, M., Shaw, G., Edwards, J.K., Desmedt, F., Miquel, P., Seuna, E., Willock, D.J., Moulijn, J.A., Hutchings, G.J., 2016. Gas phase stabiliser-free production of hydrogen peroxide using supported gold-palladium catalysts. CHEMICAL SCIENCE 7, 5833-5837.

Argyle, M.D., Bartholomew, C.H., 2015. Heterogeneous catalyst deactivation and regeneration: a review. 5, 145-269.

Bavykina, A., Kolobov, N., Khan, I.S., Bau, J.A., Ramirez, A., Gascon, J., 2020. Metal–Organic Frameworks in Heterogeneous Catalysis: Recent Progress, New Trends, and Future Perspectives. Chemical Reviews 120, 8468-8535.

Brdarić, D., Kovač-Andrić, E., Šapina, M., Kramarić, K., Lutz, N., Perković, T., Egorov, A.J.A.Q., Atmosphere, Health, 2019. Indoor air pollution with benzene, formaldehyde, and nitrogen dioxide in schools in Osijek, Croatia. 12, 963-968.

Cai, T., Wang, L., Liu, Y., Zhang, S., Dong, W., Chen, H., Yi, X., Yuan, J., Xia, X., Liu, C., Luo, S., 2018. Ag_3PO_4/Ti_3C_2 MXene interface materials as a Schottky catalyst with enhanced photocatalytic activities and anti-photocorrosion performance. Applied Catalysis B: Environmental 239, 545-554.

Cheng, J., Zhang, Z., Wang, Y., Li, F., Cao, J., Gozin, M., Ye, Y., Shen, R., 2023. Doping of Al/CuO with microwave absorbing Ti_3C_2 MXene for improved ignition and combustion performance. Chemical Engineering Journal 451, 138375.

Chu, S., Wang, E., Feng, F., Zhang, C., Jiang, J., Zhang, Q., Wang, F., Bing, L., Wang, G., Han, D., 2022. A Review of Noble Metal Catalysts for Catalytic Removal of VOCs. Catalysts 12, 1543.

Cui, C., Cheng, R., Zhang, H., Zhang, C., Ma, Y., Shi, C., Fan, B., Wang, H., Wang, X., 2020. Ultrastable MXene@ Pt/SWCNTs' nanocatalysts for hydrogen evolution reaction. Advanced Functional Materials 30, 2000693.

Deng, H., Kang, S., Ma, J., Zhang, C., He, H., 2018. Silver incorporated into cryptomelane-type Manganese oxide boosts the catalytic oxidation of benzene. Applied Catalysis B: Environmental 239, 214-222.

Espenson, J.H., 1981. Chemical kinetics and reaction mechanisms.

Gao, G., O'Mullane, A.P., Du, A., 2017. 2D MXenes: A New Family of Promising Catalysts for the Hydrogen Evolution Reaction. ACS Catalysis 7, 494-500.

Guo, Y., Sun, Y., Yang, D.-P., Dai, J., Liu, Z., Chen, Y., Huang, J., Li, Q., 2020. Biogenic $Pt/CaCO_3$ Nanocomposite as a Robust Catalyst toward Benzene Oxidation. ACS Applied Materials & Interfaces 12, 2469-2480.

Guo, Y., Yang, D.-P., Liu, M., Zhang, X., Chen, Y., Huang, J., Li, Q., Luque, R.J.J.o.M.C.A., 2019. Enhanced catalytic benzene oxidation over a novel waste-derived Ag/eggshell catalyst. 7, 8832-8844.

He, C., Cheng, J., Zhang, X., Douthwaite, M., Pattisson, S., Hao, Z., 2019. Recent Advances in the Catalytic Oxidation of Volatile Organic Compounds: A Review Based on Pollutant Sorts and Sources. Chemical Reviews 119, 4471-4568.

Heynderickx, P.M., Thybaut, J.W., Poelman, H., Poelman, D., Marin, G.B., 2009. Kinetic modeling of the total oxidation of propane over anatase and vanadia sputter deposited catalysts. Appl. Catal. B 90, 295-306.

Heynderickx, P.M., Thybaut, J.W., Poelman, H., Poelman, D., Marin, G.B., 2010a. Kinetic modeling of the total oxidation of propane over $CuO-CeO_2/\gamma-Al_2O_3$. Appl. Catal. B 95, 26-38.

Heynderickx, P.M., Thybaut, J.W., Poelman, H., Poelman, D., Marin, G.B., 2010b. The total oxidation of propane over supported Cu and Ce oxides: A comparison of single and binary metal oxides. 272, 109-120.

Huang, H., Xu, Y., Feng, Q., Leung, D.Y.C., 2015. Low temperature catalytic oxidation of volatile organic compounds: a review. Catalysis Science & Technology 5, 2649-2669.

Jiang, H., Hu, Z., Gan, C., Sun, B., Kong, S., Bian, F., 2021. Visible-light induced one-pot hydrogenation and amidation of nitroaromatics with carboxylic acids over 2D MXene-derived $Pt/N-TiO_2/Ti_3C_2$. Molecular Catalysis 504, 111490.

Jiang, Z., Zhang, W., Jin, L., Yang, X., Xu, F., Zhu, J., Huang, W., 2007. Direct XPS Evidence for Charge Transfer from a Reduced Rutile TiO_2(110) Surface to Au Clusters. The Journal of Physical Chemistry C 111, 12434-12439.

Kim, J.-M., Vikrant, K., Kim, T., Kim, K.-H., Dong, F., 2022. Thermocatalytic oxidation of gaseous benzene by a titanium dioxide supported platinum catalyst. Chemical Engineering Journal 428, 131090.

Kim, S.J., Koh, H.-J., Ren, C.E., Kwon, O., Maleski, K., Cho, S.-Y., Anasori, B., Kim, C.-K., Choi, Y.-K., Kim, J., Gogotsi, Y., Jung, H.-T., 2018. Metallic Ti_3C_2Tx MXene Gas Sensors with Ultrahigh Signal-to-Noise Ratio. ACS Nano 12, 986-993.

Kong, J., Jiang, C., Rui, Z., Liu, S., Xian, F., Ji, W., Ji, H., 2020. Photothermocatalytic synergistic oxidation: An effective way to overcome the negative water effect on supported noble metal catalysts for VOCs oxidation. Chemical Engineering Journal 397, 125485.

Konstantinova, E., Minnekhanov, A., Beltiukov, A., Ivanov, V., Sutherland, A.J., Boytsova, O.J.N.J.o.C., 2018.

Unveiling point defects in titania mesocrystals: a combined EPR and XPS study. 42, 15184-15189.
Kumar, P., Liu, J., Ranjan, P., Hu, Y., Yamijala, S.S., Pati, S.K., Irudayaraj, J., Cheng, G.J., 2018. Alpha Lead Oxide (α-PbO): A New 2D Material with Visible Light Sensitivity. Small 14, 1703346.
Lelicińska-Serafin, K., Rolewicz-Kalińska, A., Manczarski, P., 2019. VOC Removal Performance of a Joint Process Coupling Biofiltration and Membrane-Filtration Treating Food Industry Waste Gas. International Journal of Environmental Research and Public Health 16.
Lhuissier, M., Couvert, A., Dabert, P., Amrane, A., Kane, A., Audic, J.-L., Dumont, E., 2022. Removal of a Mixture of Seven Volatile Organic Compounds (VOCs) Using an Industrial Pilot-Scale Process Combining Absorption in Silicone Oil and Biological Regeneration in a Two-Phase Partitioning Bioreactor (TPPB). Energies 15.
Li, J., Tang, W., Liu, G., Li, W., Deng, Y., Yang, J., Chen, Y., 2016. Reduced graphene oxide modified platinum catalysts for the oxidation of volatile organic compounds. Catalysis Today 278, 203-208.
Li, X., Pillai, S.C., Wei, L., Liu, Z., Huang, L., Huang, Q., Jia, X., Hou, D., Song, H., Wang, H., 2020a. Facile synthesis of polyoxometalate-modified metal organic frameworks for eliminating tetrabromobisphenol-A from water. Journal of Hazardous Materials 399, 122946.
Li, X., Zhang, L., Yang, Z., Wang, P., Yan, Y., Ran, J., 2020b. Adsorption materials for volatile organic compounds (VOCs) and the key factors for VOCs adsorption process: A review. Separation and Purification Technology 235, 116213.
Li, Y., Chen, T., Zhao, S., Wu, P., Chong, Y., Li, A., Zhao, Y., Chen, G., Jin, X., Qiu, Y., Ye, D., 2022. Engineering Cobalt Oxide with Coexisting Cobalt Defects and Oxygen Vacancies for Enhanced Catalytic Oxidation of Toluene. ACS Catalysis 12, 4906-4917.
Liu, B., Younis, S.A., Kim, K.-H., 2021. The dynamic competition in adsorption between gaseous benzene and moisture on metal-organic frameworks across their varying concentration levels. Chemical Engineering Journal 421, 127813.
Liu, L., Zhao, Q., Liu, R., Zhu, L., 2019. Hydrogen adsorption-induced catalytic enhancement over Cu nanoparticles immobilized by layered Ti_3C_2 MXene. Applied Catalysis B: Environmental 252, 198-204.
Matsumoto, K., Hiyoshi, M., Iijima, T., Noguchi, H., Uosaki, K., 2020. Investigation of the effects of Pt/Pd composition and PVP content on the activity of Pt/Pd core-shell catalysts. Electrochemistry Communications 115, 106736.
Nan, J., Guo, X., Xiao, J., Li, X., Chen, W., Wu, W., Liu, H., Wang, Y., Wu, M., Wang, G., 2021. Nanoengineering of 2D MXene-Based Materials for Energy Storage Applications. Small 17, 1902085.
Obodo, K.O., Ouma, C.N.M., Modisha, P.M., Bessarabov, D., 2020. Density functional theory calculation of Ti_3C_2 MXene monolayer as catalytic support for platinum towards the dehydrogenation of methylcyclohexane. Applied Surface Science 529, 147186.
Panov, G.I., Dubkov, K.A., Starokon, E.V., 2006. Active oxygen in selective oxidation catalysis. Catalysis Today 117, 148-155.
Parse, H., Patil, I.M., Swami, A.S., Kakade, B.A., 2021. TiO_2-Decorated Titanium Carbide MXene co-Doped with Nitrogen and Sulfur for Oxygen Electroreduction. ACS Applied Nano Materials 4, 1094-1103.
Petrusová, Z., Machanová, K., Stanovský, P., Izák, P., 2019. Separation of organic compounds from gaseous mixtures by vapor permeation. Separation and Purification Technology 217, 95-107.
Poerwoprajitno, A.R., Gloag, L., Watt, J., Cheong, S., Tan, X., Lei, H., Tahini, H.A., Henson, A., Subhash, B., Bedford, N.M., Miller, B.K., O'Mara, P.B., Benedetti, T.M., Huber, D.L., Zhang, W., Smith, S.C., Gooding, J.J., Schuhmann, W., Tilley, R.D., 2022. A single-Pt-atom-on-Ru-nanoparticle electrocatalyst for CO-resilient methanol oxidation. Nature Catalysis 5, 231-237.
Qin, L., Huang, X., Zhao, B., Wang, Y., Han, J., 2020. Iron Oxide as a Promoter for Toluene Catalytic Oxidation Over Fe–Mn/γ-Al_2O_3 Catalysts. Catalysis Letters 150, 802-814.
Ran, J., Gao, G., Li, F.-T., Ma, T.-Y., Du, A., Qiao, S.-Z., 2017. Ti_3C_2 MXene co-catalyst on metal sulfide photo-absorbers for enhanced visible-light photocatalytic hydrogen production. Nature Communications 8, 13907.
Rosli, S.N.A., Abidin, S.Z., Osazuwa, O.U., Fan, X., Jiao, Y., 2022. The effect of oxygen mobility/vacancy on carbon gasification in nano catalytic dry reforming of methane: A review. Journal of CO2 Utilization 63, 102109.
Roy, K., Verma, K.M., Vikrant, K., Goswami, M., Sonwani, R.K., Rai, B.N., Vellingiri, K., Kim, K.-H., Giri, B.S., Singh, R.S., 2018. Removal of Patent Blue (V) Dye Using Indian Bael Shell Biochar: Characterization, Application and Kinetic Studies. Sustainability 10, 2669.
Saqlain, S., Cha, B.J., Kim, S.Y., Sung, J.Y., Choi, M.C., Seo, H.O., Kim, Y.D., 2021. Impact of humidity on the removal of volatile organic compounds over Fe loaded TiO_2 under visible light irradiation: Insight into photocatalysis mechanism by operando DRIFTS. Materials Today Communications 26, 102119.
Sekar, A., Varghese, G.K., Ravi Varma, M.K., 2019. Analysis of benzene air quality standards, monitoring methods and concentrations in indoor and outdoor environment. Heliyon 5, e02918.

Shim, W.G., Kim, S.C., 2010. Heterogeneous adsorption and catalytic oxidation of benzene, toluene and xylene over spent and chemically regenerated platinum catalyst supported on activated carbon. Applied Surface Science 256, 5566-5571.
Sophiana, I.C., Topandi, A., Iskandar, F., Devianto, H., Nishiyama, N., Budhi, Y.W., 2020. Catalytic oxidation of benzene at low temperature over novel combination of metal oxide based catalysts: CuO, MnO_2, NiO with $Ce_{0.75}Zr_{0.25}O_2$ as support. Materials Today Chemistry 17, 100305.
Sun, H., Liu, Z., Chen, S., Quan, X., 2015. The role of lattice oxygen on the activity and selectivity of the OMS-2 catalyst for the total oxidation of toluene. Chemical Engineering Journal 270, 58-65.
Tran, T.Y., Younis, S.A., Heynderickx, P.M., Kim, K.-H., 2022. Validation of two contrasting capturing mechanisms for gaseous formaldehyde between two different types of strong metal-organic framework adsorbents. Journal of Hazardous Materials 424, 127459.
Vikrant, K., Kim, K.-H., Dong, F., Boukhvalov, D.W., Choi, W., 2022. Deep oxidation of gaseous formaldehyde at room-temperature by a durable catalyst formed through the controlled addition of potassium to platinum supported on waste eggshell. Chemical Engineering Journal 428, 131177.
Vikrant, K., Kim, K.-H., Peng, W., Ge, S., Sik Ok, Y., 2020. Adsorption performance of standard biochar materials against volatile organic compounds in air: A case study using benzene and methyl ethyl ketone. Chemical Engineering Journal 387, 123943.
Vikrant, K., Kim, K.-H., Szulejko, J.E., Pandey, S.K., Singh, R.S., Giri, B.S., Brown, R.J.C., Lee, S.H., 2017. Bio-filters for the Treatment of VOCs and Odors-A Review. Asian Journal of Atmospheric Environment 11, 139-152.
Vikrant, K., Weon, S., Kim, K.-H., Sillanpää, M., 2021. Platinized titanium dioxide (Pt/TiO_2) as a multi-functional catalyst for thermocatalysis, photocatalysis, and photothermal catalysis for removing air pollutants. Applied Materials Today 23, 100993.
Vikrant, K., Yang, H., Chung, M.W., Kim, K.H., Dong, F., Weon, S., He, C., Heynderickx, P.M., 2023. Two-dimensional titanium carbide (MXene)-supported Pt_3Ti intermetallic compound catalysts for efficient room-temperature oxidative removal of gaseous formaldehyde. Materials Today Nano 21, 100283.
Vyazovkin, S., 2021. Determining preexponential factor in model-free kinetic methods: How and why? Molecules 26, 3077.
Wang, Y., Yang, D., Li, S., Zhang, L., Zheng, G., Guo, L., 2019. Layered copper manganese oxide for the efficient catalytic CO and VOCs oxidation. Chemical Engineering Journal 357, 258-268.
Xu, R., Dai, C., Mu, M., Cheng, J., Lei, Z., Wu, B., Liu, N., Chen, B., Yu, G., 2021a. Highly efficient capture of odorous sulfur-based VOCs by ionic liquids. Journal of Hazardous Materials 402, 123507.
Xu, W., Chen, X., Chen, J., Jia, H., 2021b. Bimetal oxide CuO/Co_3O_4 derived from Cu ions partly-substituted framework of ZIF-67 for toluene catalytic oxidation. Journal of Hazardous Materials 403, 123869.
Yang, C., Miao, G., Pi, Y., Xia, Q., Wu, J., Li, Z., Xiao, J., 2019. Abatement of various types of VOCs by adsorption/catalytic oxidation: A review. Chemical Engineering Journal 370, 1128-1153.
Yang, X., Liu, S., Li, J., Chen, J., Rui, Z., 2020. Promotion effect of strong metal-support interaction to thermocatalytic, photocatalytic, and photothermocatalytic oxidation of toluene on $Pt/SrTiO_3$. Chemosphere 249, 126096.
Zhan, W., Ma, L., Gan, M., 2022. In-situ growth of CoP wrapped by carbon nanoarray-like architecture onto nitrogen-doped Ti_3C_2 Pt-based catalyst for efficient methanol oxidation. Materials Today Chemistry 26, 101041.
Zhang, C., Wang, Y., Li, G., Chen, L., Zhang, Q., Wang, D., Li, X., Wang, Z., 2020. Tuning smaller Co3O4 nanoparticles onto HZSM-5 zeolite via complexing agents for boosting toluene oxidation performance. Applied Surface Science 532, 147320.
Zhang, X., Junhui, Y., Jing, Y., Ting, C., Bei, X., Zhe, L., Kunfeng, Z., Ling, Y., Dannong, H., 2018. Excellent low-temperature catalytic performance of nanosheet Co-Mn oxides for total benzene oxidation. Applied Catalysis A: General 566, 104-112.
Zhang, X., Xu, S., Li, Q., Zhou, G., Xia, H., 2021. Recent advances in the conversion of furfural into bio-chemicals through chemo- and bio-catalysis. RSC Advances 11, 27042-27058.
Zhang, Y., Zhou, J.J.J.o.C., 2021. Synergistic catalysis by a hybrid nanostructure Pt catalyst for high-efficiency selective hydrogenation of nitroarenes. 395, 445-456.
Zhang, Z., Jiang, Z., Shangguan, W.J.C.T., 2016. Low-temperature catalysis for VOCs removal in technology and application: A state-of-the-art review. 264, 270-278.
Zhao, X., Xu, D., Wang, Y., Zheng, Z., Li, K., Zhang, Y., Zhan, R., Lin, H., 2021. Electric field assisted benzene oxidation over Pt-Ce-Zr nano-catalysts at low temperature. Journal of Hazardous Materials 407, 124349.
Zhu, S., Xie, X., Chen, S.-C., Tong, S., Lu, G., Pui, D.Y., Sun, J.J.A.S.S., 2017. Cu-Ni nanowire-based TiO_2 hybrid for the dynamic photodegradation of acetaldehyde gas pollutant under visible light. 408, 117-124.

659

660 **Tables and Figures**

Table 1. The benzene removal performance of the tested catalysts.[a]

Order	Catalyst	T_{50} (°C)[b]	T_{90} (°C)[c]	T_{100} (°C)[d]	r (mol g_{cat}^{-1} h^{-1})[e]	r (mol g_{Pt}^{-1} h^{-1})[f]
1	Ti_3C_2-R	–	–	–	0.001	-
2	1% Pt@Ti_3C_2	195	230	325	0.007	0.82
3	1% Pt@Ti_3C_2-R	167	191	225	0.012	1.27
4	0.1 %Pt@Ti_3C_2-R	207	255	350	0.005	3.96
5	2% Pt@Ti_3C_2-R	139	162	200	0.012	0.58

[a] Reactant composition: benzene (10 ppm) + air (balance), FR: 50 mL·min^{-1}, mass: 10 mg MXene + 50 mg sands, and reduction pre-treatment (under the flow (50 mL·min^{-1}) of 10% H_2/N_2 at 300 °C for 3 h).
[b] Reaction temperature at 50% $R_{benzene}$.
[c] Reaction temperature at 90% $R_{benzene}$.
[d] Reaction temperature at 100% $R_{benzene}$.
[e] Reaction rate per catalyst mass obtained at 200 °C.
[f] Reaction rate per Pt mass obtained at 200 °C.

661

662

Table 2. The ratio of the lattice oxygen, adsorbed oxygen, Pt^0, and Pt^{2+} of tested materials (analysis by XPS).

Order	Catalyst	Lattice oxygen (O^*)	Adsorbed oxygen (O_{ads})	Pt^0	Pt^{2+}
1	1% Pt@Ti_3C_2	45.3%	54.7%	65.4%	34.6%
2	1% Pt@Ti_3C_2-R	71.0%	29.0%	38.9%	61.1%
3	1% Pt@Ti_3C_2-R (after reaction)	63.0%	37.0%	59.5%	40.5%

663
664

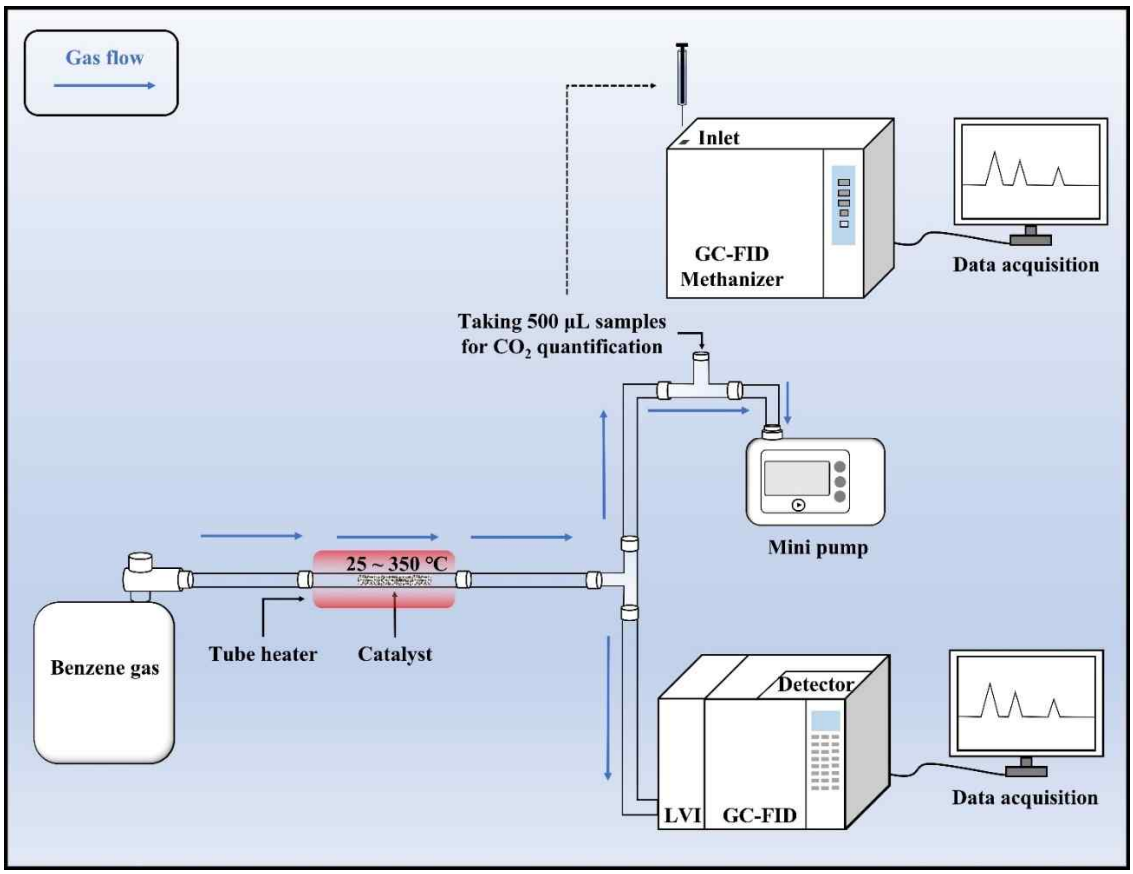

Figure 1. Schematic of the benzene catalytic oxidation experimental setup.

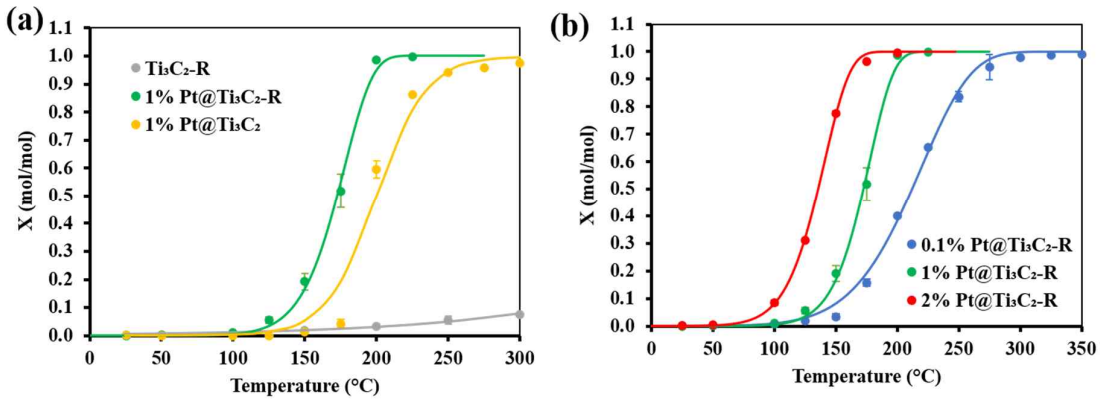

Figure 2. Light-off curves for the conversion performance of benzene (10 ppm in dry air and RH = 0%): (a) comparison between the catalysts of the control group (bed mass: 10 mg catalyst + 50 mg sand and FR: 50 mL·min^{-1}) and (b) effect of different platinum loading (bed mass: 10 mg catalyst + 50 mg sand and FR: 50 mL·min^{-1}) on Pt@Ti_3C_2-R.

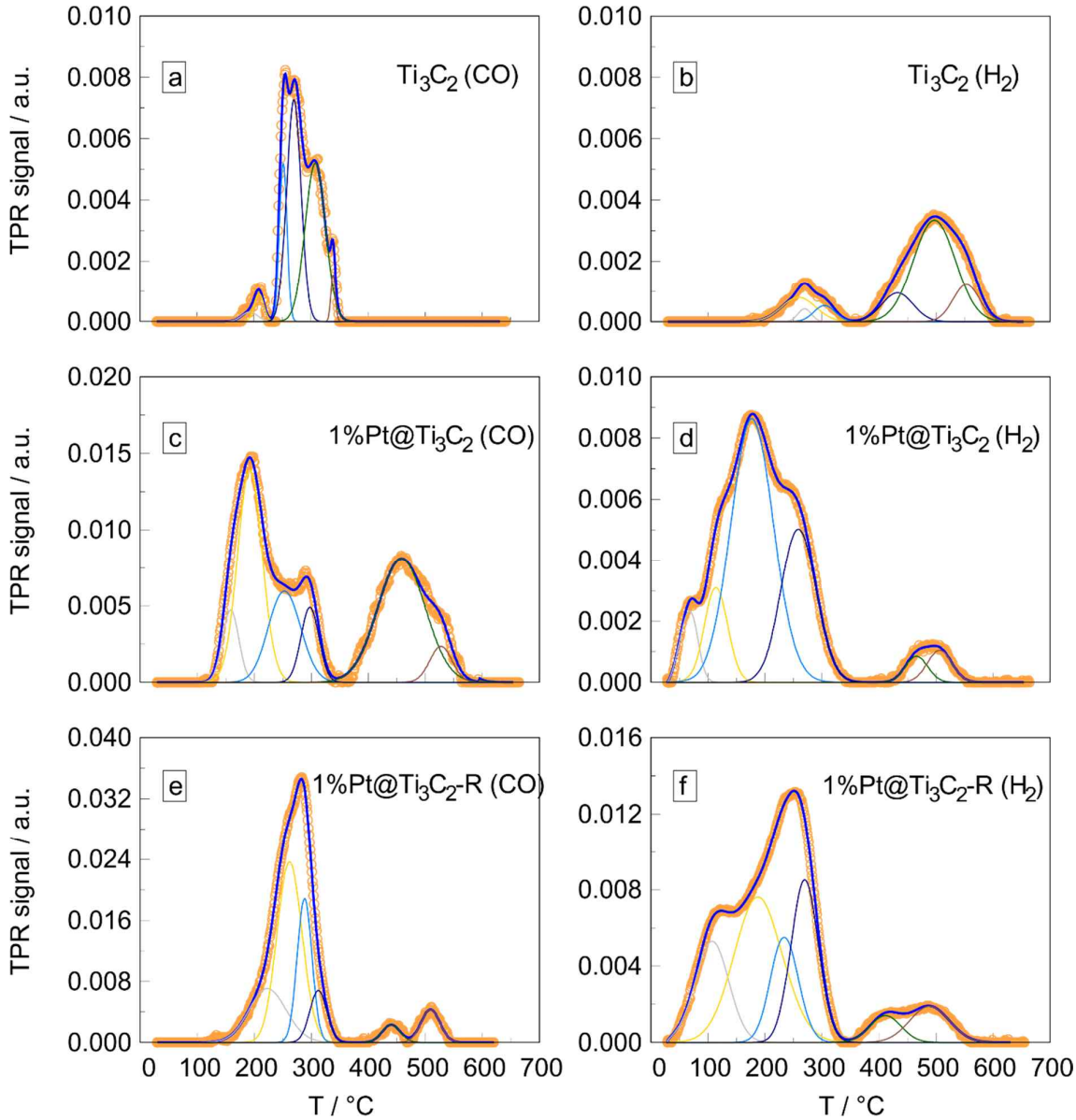

Figure 3. TPR analysis (profiles =○) of the tested materials: (a) Ti_3C_2 (under CO), (b) Ti_3C_2 (under H_2), (c) 1%Pt@Ti_3C_2 (under CO), (d) 1%Pt@Ti_3C_2 (under H_2), (e) 1%Pt@Ti_3C_2-R (under CO), and (f) 1%Pt@Ti_3C_2-R (under H_2). Gaussian model, according to Equation S2, for peak 1 (—), peak 2 (—), peak 3 (—), peak 4 (—),peak 5 (—), peak 6 (—), and total calculated signal (—). The ramp rate was 10 K/min.

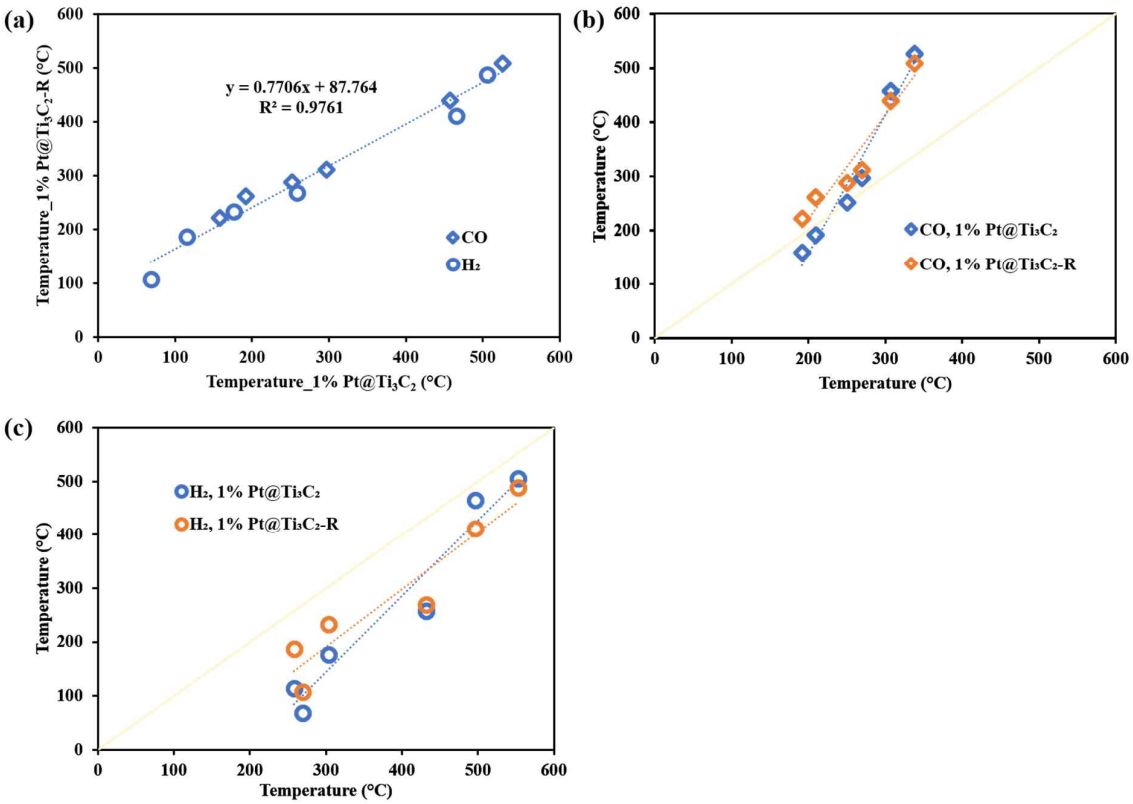

Figure 4. Comparisons of peak temperatures of 1% Pt@Ti_3C_2 and 1% Pt@Ti_3C_2-R based on TPR analysis: (a) CO (□) and H_2 (○). (b) CO results between 1% Pt@Ti_3C_2 (□) versus 1% Pt@Ti_3C_2-R (□). (c) H_2 results between 1% Pt@Ti_3C_2 (○) versus 1% Pt@Ti_3C_2-R (○).

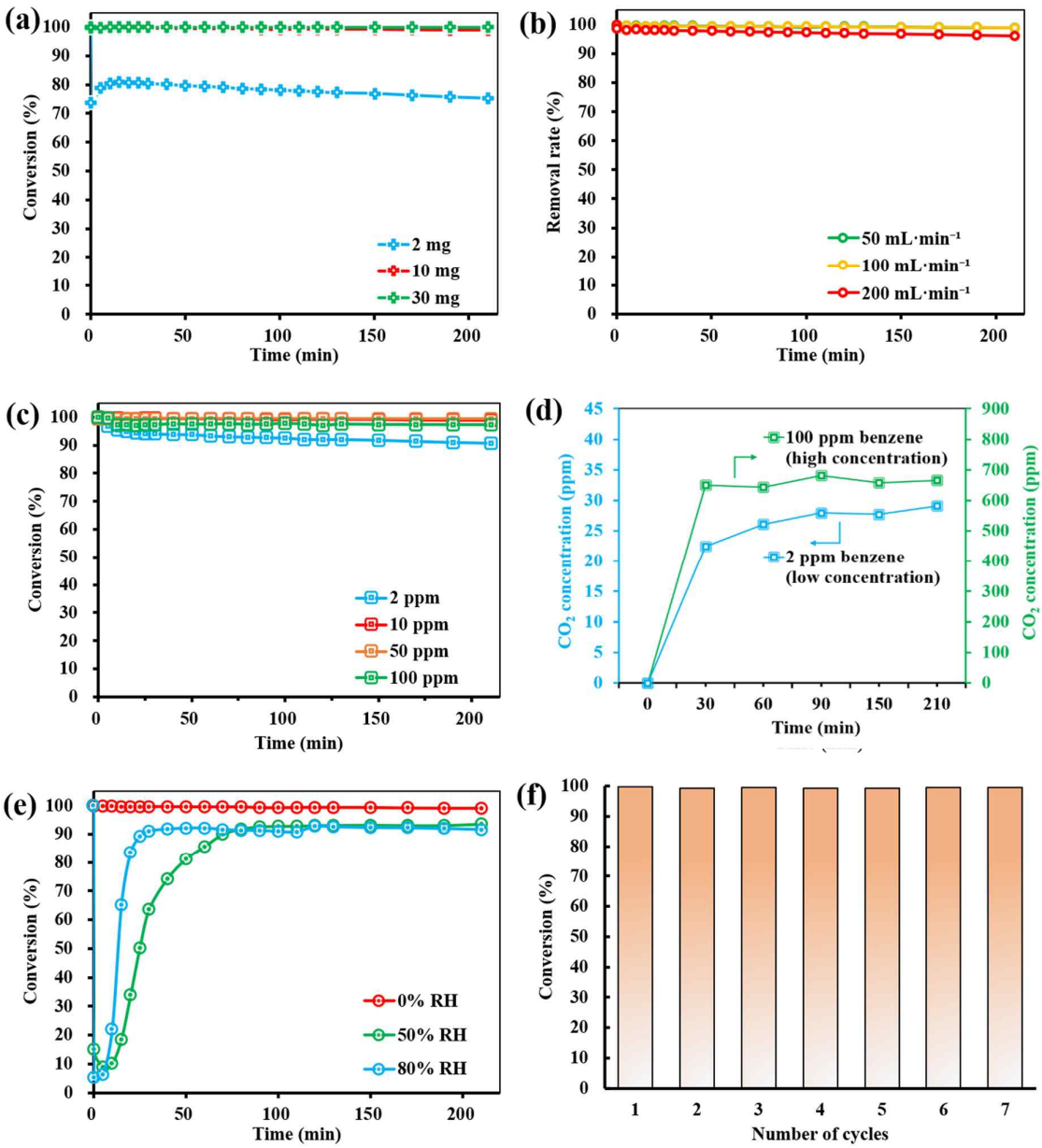

Figure 5. The effects of process variables on the catalytic activity of 1% Pt@Ti_3C_2-R (bed mass: 10 mg catalyst + 50 mg sand) against benzene at a gaseous FR of 50 mL·min^{-1}: (a) effect of bed mass (bed mass: 2□30 mg catalyst mixed with sands (at a fixed weight ratio of 1:5), benzene: 10 ppm, and FR: 50 mL·min^{-1}), (b) effect of FR (bed mass: 10 mg catalyst + 50 mg sand and 10 ppm benzene), (c) effect of benzene concentrations (2□100 ppm) at RH= 0%, (d) CO_2 yield at benzene concentration of 2 and 100 ppm (in air) and RH: 0%, (e) effect of RH (0%, 50%, and 80%) against 10 ppm benzene oxidation (in air), and (f) recycle test against 10 ppm benzene oxidation (in dry air; RH: 0%).

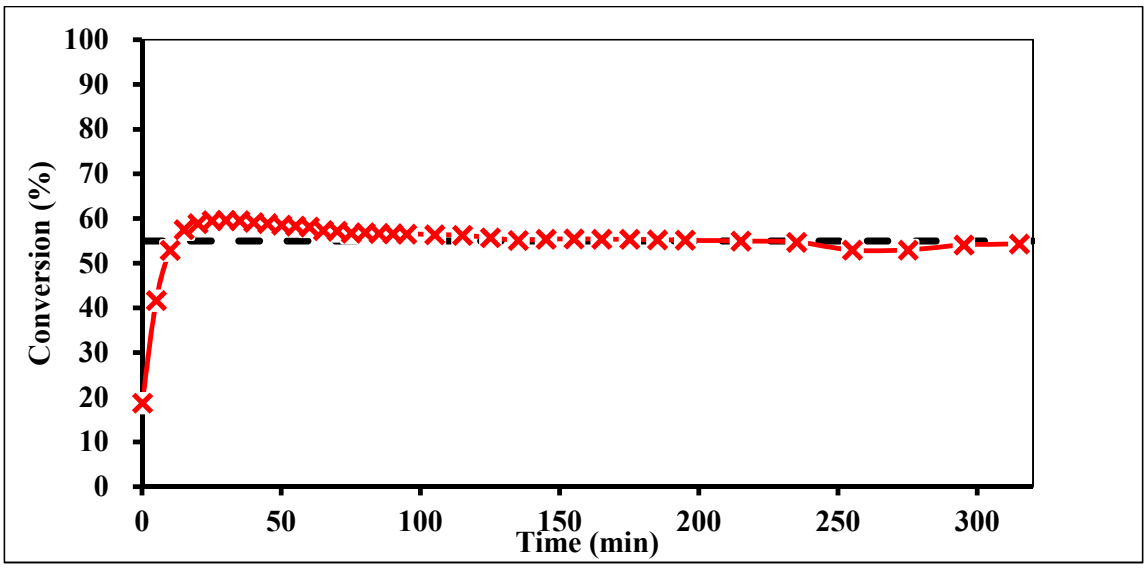

Figure 6. Benzene oxidation stability test of 1% Pt@Ti_3C_2-R (mass: 2 mg catalyst + 10 mg sand, benzene concentration: 10 ppm (in dry air, RH: 0%), FR: 50 mL·min^{-1}, and reaction temperature: 200 °C).

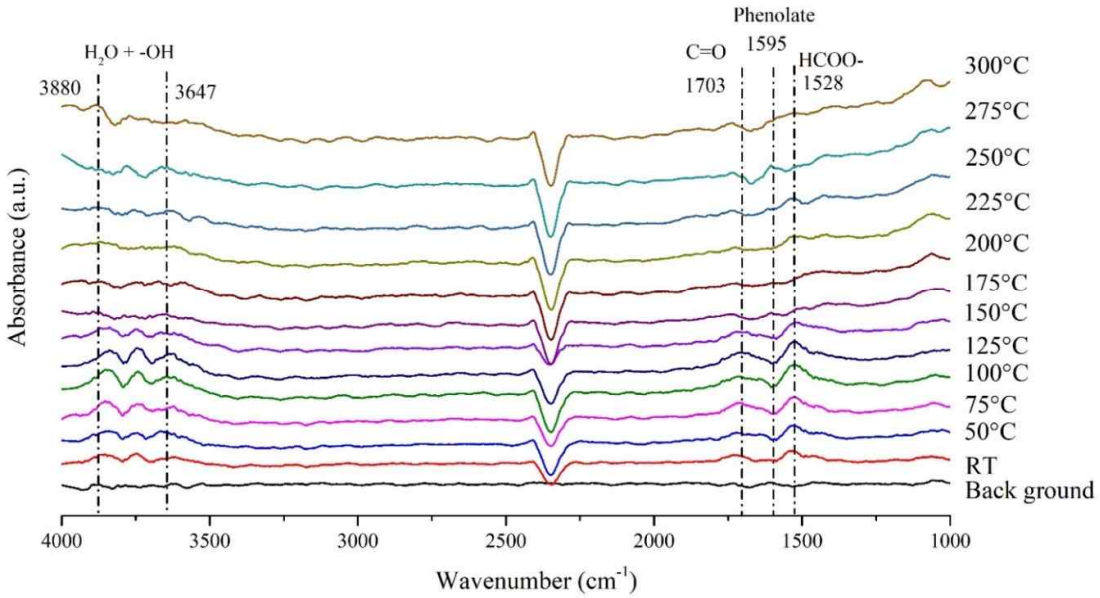

Figure 7. In situ DRIFTS spectra over 1% Pt@Ti_3C_2-R at RT–300 °C (benzene + air, 1:1 mixture).